Prediction of Dynamical Properties of Biochemical Pathways with Graph Neural Networks

Pasquale Bove, Alessio Micheli, Paolo Milazzo and Marco Podda
Department of Computer Science, University of Pisa, Largo B. Pontecorvo, 3, 56127, Pisa, Italy

Keywords: Systems Biology, Pathway Modelling, Robustness, Deep Learning, Graph Neural Networks.

Abstract: Biochemical pathways are often represented as graphs, in which nodes and edges give a qualitative description of the modeled reactions, while node and edge labels provide quantitative details such as kinetic and stoichiometric parameters. Dynamical properties of biochemical pathways are usually assessed by performing numerical (ODE-based) or stochastic simulations in which quantitative parameters are essential. These simulation methods are often computationally very expensive, in particular when property assessment requires varying parameters such as initial concentrations of molecules. In this paper we propose the use of a Deep Neural Network (DNN) to predict such dynamical properties relying only on the graph structure. In particular, our model is based on Graph Neural Networks. We focus on the dynamical property of concentration robustness, which is the ability of the pathway to maintain the concentration of some molecules within certain intervals despite of perturbation in the initial concentration of other molecules. The use of DNNs can allow robustness to be predicted by avoiding the burden of performing a huge number of numerical or stochastic simulations. Moreover, once trained, the model could be applied to predicting robustness properties for pathways in which quantitative parameters are not available.

1 INTRODUCTION

In order to understand the mechanisms underlying the functioning of living cells, it is necessary to analyze their activities at the biochemical level. Biochemical pathways (or networks) are complex dynamical systems in which molecules interact with each other through chemical reactions. In these reactions, molecules can take different roles: reactant, product, promoter and inhibitor.

Chemical kinetics laws, such as the law of mass action, allow describing and analysing the dynamics of a set of chemical reactions through Ordinary Differential Equations (ODEs). Moreover, stochastic modelling and simulation approaches, typically based on one of the many variants of Gillespie's simulation algorithm (Gillespie, 1977) are often adopted in the case of pathways involving molecules available in small concentrations, which make the dynamics of reactions sensitive to random events.

Biochemical pathways are very often represented as graphs. Many different graphical notations exist (see, e.g., Karp and Paley (1994); Reddy et al. (1993); Le Novere et al. (2009)). Most of them essentially represent molecules as nodes and reactions as multi-edges or as additional nodes. Graphical notations are very common since they provide a quite natural visual representation of the involved reactions. These notations enable network and structural analysis methods to be applied to the investigation of properties of the pathway as a whole. Moreover, they can usually be translated into ODEs or stochastic models in order to apply standard numerical simulation techniques.

Models of biochemical pathways are typically used to investigate dynamical properties of these systems such as the reachability of steady states, the occurrence of oscillatory behaviors, causalities between species, and robustness. The assessment of these properties often requires the execution of several numerical or stochastic simulations. In particular, robustness (Kitano, 2004), i.e. the maintenance of some concentration levels against the perturbation of parameters or initial conditions, is a key property of many biochemical pathways. Its assessment usually requires a huge number of simulations in order to extensively explore the parameter space.

This paper aims at investigating the applicability of Machine Learning (ML), and in particular Deep Learning (Goodfellow et al., 2016) methods for graphs to the prediction of dynamical properties of

Bove, P., Micheli, A., Milazzo, P. and Podda, M.
Prediction of Dynamical Properties of Biochemical Pathways with Graph Neural Networks.
DOI: 10.5220/0008964700320043
In *Proceedings of the 13th International Joint Conference on Biomedical Engineering Systems and Technologies (BIOSTEC 2020) - Volume 3: BIOINFORMATICS*, pages 32-43
ISBN: 978-989-758-398-8; ISSN: 2184-4305

biochemical pathways. The assumption at the basis of this study is that some dynamical properties of pathways could be correlated with topological properties of the graphs modeling such pathways. The idea is then to use ML methods to automatically infer those topological properties in a dataset of pathway graphs, and predict the dynamical property of interest on their basis. Labels in the dataset are determined by performing numerical simulations based on ODE models of the associated pathways. If the initial assumption is correct, the obtained ML model could be able to predict whether the studied dynamical property holds, thus reducing the need of performing expensive numerical or stochastic simulations. Moreover, once trained the ML model could be applied to predicting dynamical properties of pathways for which quantitative parameters are not available. To our knowledge, this is the first work that addresses this open challenge, in contrast with many approaches in literature that mainly focus on inferring the parameters of a single pathway or the relationships between its species. In summary, we test the strong assumption that network structure alone is sufficient to predict dynamical properties of pathways, and verify experimentally to which extent it is.

In this study, we focus on the assessment of the dynamical property of robustness (Kitano, 2004) on the basis of a graph representation of biochemical pathways in terms of Petri nets (Reddy et al., 1993). We start from the creation of a dataset of Petri nets obtained from curated pathway models in SBML format downloaded from the BioModels[1] database (Li et al., 2010). Robustness indicators of these pathways (to be used as labels in the dataset) have been computed by performing ODE-based simulations using the `libRoadRunner` Python library (Somogyi et al., 2015), which exploits GPU computing power. In particular, given a pathway model and a pair of molecular species (called input and output species), the computed robustness value measures how much the concentration of the output species at the steady state is influenced by perturbations of the initial concentration of the input species. This is a notion of *concentration robustness* (Shinar and Feinberg, 2010) which is to some extent correlated with the notion of global sensitivity (Zi, 2011). To predict the robustness indicators associated to pairs of input/output species of a given pathway, we propose the following framework: first, we construct a subgraph of the pathway, which contains the input and output node as well as all the nodes that influence the reaction dynamics. Then, we develop a Deep Neural Network (DNN) model composed of two modules trained jointly: a Graph Neural Network (GNN) (Scarselli et al., 2009; Micheli, 2009) that processes the subgraph, automatically extracting structural information that correlate with its robustness in the form of a vector; and a Multi-Layer Perceptron (Murtagh, 1991) predictor which, given the vectorial representation inferred by the GNN, classifies the graph as robust or not. We assess the performances of this model on out-of-sample (unseen during training) data, showing that we are indeed able to predict robustness with reasonable accuracy. The rest of the paper is structured as follows. Section 2 contains some background notions of robustness and Petri nets modeling of pathways. In Section 3 we describe our methodology, defining the predictive task as well as providing details of the Deep Neural Network model. Section 4 describes the experimental setup. In Section 5 we discuss the results of our experiments. Finally, in Section 6 we draw our conclusions and discuss future work.

[1]BioModels: https://www.ebi.ac.uk/biomodels/

2 BACKGROUND

2.1 Biological Robustness

Robustness is a property observed in many biological systems. It is the ability of the system to maintain its functionalities again external and internal perturbations (Kitano, 2004). A general formalization of the notion of robustness has been proposed in (Kitano, 2007), where the robustness R of a system s with regard to a specific functionality a and against a set of perturbations P is defined as:

$$R^s_{a,P} = \int_P \psi(p) D^s_a(p) dp$$

In this definition, $\psi(p)$ is the probability for perturbation p to take place, and $D_a(p)$ is a relative evaluation function for functionality a under perturbation p. Let the *viability* of a functionality to be a measure of the ability of the cell to carry out it. This could be expressed, for instance, in terms of the synthesis/degradation rate or concentration level of some target substance, in terms of cell growth rate, or in terms of any other suitable quantitative indicator. Function $D_a(p)$ gives the viability of a under perturbation p relative to the viability of the same functionality in normal conditions. By assuming that in the absence of perturbations functionality a is carried out in an optimal way, we have $D_a(p) = 0$ for perturbations causing the system to fail in a, $D_a(p) = 1$ in the cases of no or irrelevant perturbations (i.e. having no influence), and $0 < D_a(p) < 1$ in the case of relevant perturbations.

Kitano's formulation of robustness has been improved in (Rizk et al., 2009), where functionalities to be maintained are described as linear temporal logic (LTL) formulas and the impact of perturbations is measured through a notion of *violation degree* measuring the distance between the dynamics of the perturbed system and the LTL formula. Many more specific definitions exist, which differ either in the class of biological systems they apply to, or in the way the functionality to be maintained is expressed (Larhlimi et al., 2011). In the case of biochemical pathways, robustness can be expressed in terms of maintenance of the concentration of some species in the steady state against perturbations in the kinetic parameters or in the initial concentration of some other species. This is formally expressed by the notion of *absolute concentration robustness* proposed in (Shinar and Feinberg, 2010).

A generalization of absolute concentration robustness, called α-*robustness*, has been proposed in (Nasti et al., 2018), where concentration intervals are considered both for the perturbed molecules (input species) and for the molecules whose concentration is maintained (output species). Roughly speaking, a biochemical pathway is α-robust with respect to a given set of initial concentration intervals if the concentration of a chosen output molecule at the steady state varies within an interval of values $[k-\alpha/2, k+\alpha/2]$ for some $k \in \mathbb{R}$. A relative version of α-robustness can be obtained simply by dividing α by k. The notion of α-robustness is related with the notion of global sensitivity (Zi, 2011) which typically measures the average effect of a set of perturbations.

Assessment of robustness properties is usually obtained by performing exhaustive (in the parameter space) numerical simulations (Rizk et al., 2009; Iooss and Lemaître, 2015). In some particular cases there exist sufficient conditions on the biological network structure that can avoid simulations to be performed (Shinar and Feinberg, 2010). Moreover, the assessment of monotonicity properties in the dynamics of the network may allow the number of simulations to be significantly reduced (Gori. et al., 2019).

2.2 Petri Nets Modeling of Pathways

Biochemical pathways are essentially sets of chemical reactions. A chemical reaction can be described by a multiset of *reactants*, a multiset of *products*, and the *kinetic constant* of the reaction. Reactants and products are multisets since more than one instance of the same molecule could be consumed or produced by a reaction. Moreover, according to the standard chemical law of mass action, the rate of occurrence of the reaction is given by its kinetic constant multiplied by the concentrations of its reactants in considered chemical solution. For example, let us assume A and B to be molecules and let us use the same symbols A and B to denote the respective concentrations in kinetic formulas. We have that $A + B \xrightarrow{k} 2B$ describes the chemical reaction in which reactants A and B are transformed into two instances of B (the products) at a rate given by the kinetic formula kAB (as is happens, for example, in Lotka-Volterra reactions).

In the context of biochemistry (and of biochemical pathways) reactions are described at a higher level of abstraction, by allowing the modeler to include in their description molecules that act either as *promoter* or as *inhibitor*. This means that there are additional molecules associated with reactions, that are not listed among reactants and products, but which may have a role in the kinetic formula (that now could no longer follow the mass action principle).

For example, in the SBML language (Hucka et al., 2018), a standard XML-based modeling language for biochemical pathways, each reaction can be associated with a number of *modifiers* the concentration of which can be used in the kinetic formula of the reaction. In Figure 1a we show a table describing a biochemical pathway as a set of reactions (first column). Each reaction is associated with its kinetic formula (third column). Moreover, a couple of reactions are associated with a modifier (second column), namely A and F. From the kinetic formulas of those two reactions it is clear that A acts as a promoter of reaction $C + D \to E$ (the rate is proportional to the concentration of A) and that F acts as inhibitor of reaction $G \to H$ (the rate is inversely proportional to the concentration of F). Kinetic formulas can then be used to construct a system of Ordinary Differential Equations (ODEs) as shown in Figure 1b.

A graphical representation of biochemical pathways can be given in terms of Petri nets (Reddy et al., 1993; Gilbert et al., 2007). Petri nets have been originally proposed as a formalism of the description and analysis of concurrent systems (Peterson, 1977), but later have been adopted for the modeling of other kinds of systems, such as biological ones. Several variants of Petri nets exist. For the aim of this work we consider a version of *continuous* Petri nets (Gilbert et al., 2007) with promotion and inhibition arcs and general kinetic functions. We call this variant *pathway Petri nets*.

A pathway Petri net is essentially a bipartite graph with different types of arcs and with labels in both edges and arcs. According to standard Petri nets terminology, the two types of edges are called *places* and *transitions*. The dynamics (or semantics) of a Petri

Reaction	*Mod*	*Kinetics*
$A+B \to 2B$		k_1AB
$B \to A$		k_2B
$C+D \to E$	A	k_3CDA
$E \to F$		k_4E
$F \to E$		k_5F
$G \to H$	F	$\frac{k_6G}{1+2F}$
$H \to G$		k_7G

(a) Reactions

$$\frac{dA}{dt} = -k_1AB + k_2B$$
$$\frac{dB}{dt} = k_1AB - k_2B$$
$$\frac{dC}{dt} = -k_3CDA$$
$$\frac{dD}{dt} = -k_3CDA$$
$$\frac{dE}{dt} = k_3CDA - k_4E + k_5F$$
$$\frac{dF}{dt} = k_4E - k_5F$$
$$\frac{dG}{dt} = -\frac{k_6G}{1+2F} + k_7G$$
$$\frac{dH}{dt} = \frac{k_6G}{1+2F} - k_7G$$

(b) ODEs

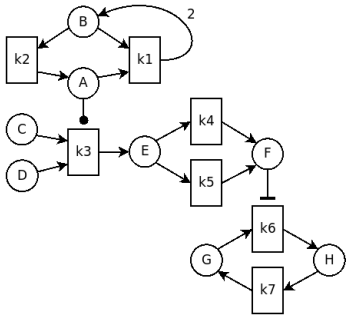

(c) Pathway Petri net

Figure 1: Example of biochemical pathway: list of reactions with information on modifiers and kinetic formulas (as they can be obtained from a SBML model), corresponding ODE model and pathway Petri net.

net in a continuous setting is described by a system of ODEs with one equation for each place. In the case of pathways, such a system of ODEs corresponds exactly to the one that can be obtained from the modeled chemical reactions (as in Figure 1b). A state of a pathway Petri net (called *marking*) is then an assignment of positive real values to the variables of the ODEs. We denote with M the set of all possible markings.

A *pathway Petri net* can be formally defined as a tuple $N = (P, T, f, p, h, v, m_0)$ where:

- P and T are finite, non empty, disjoint sets of *places* and *transitions*, respectively;
- $f : ((P \times T) \cup (T \times P)) \to \mathbb{N}^{\geq 0}$ defines the set of *directed arcs*, weighted by non-negative integer values;
- $p, h \subseteq (P \times T)$ are the sets of *promotion* and *inhibition* arcs;
- $v : T \to \Psi$, with $\Psi = M \to \mathbb{R}^{\geq 0}$, is a function that assigns to each transition a function corresponding to the computation of a kinetic formula to every possible marking $m \in M$;
- $m_0 \in M$ is the initial marking.

The visual representation of a pathway Petri net is shown in Figure 1c, that is the net corresponding to the pathway in Figure 1a. Places P and transitions T of a pathway Petri net represent molecules and reactants, and are depicted as circles and rectangles, respectively. In the figure, places contain the name of the corresponding molecule. Directed arcs f, depicted as standard arrows, connect reactants to reactions and reactions to products. The weight of such arcs (omitted if 1) correspond to the multiplicity (i.e. stoichiometry) of the connected molecules as reactant/product of the reaction. If 0 the whole arc is omitted. Promotion and inhibition arcs, p and h, connect molecules to the reactions they promote or inhibit, respectively, and they are depicted as arrows ended by a filled dot or a T. The kinetic formulas (actually, only the constants k_i, for the sake of readability) described by the labeling function v are shown inside the rectangles of the corresponding transitions. We assume molecules connected through promotion arcs to give a positive contribution to the value of the kinetic formula, while molecules connected through inhibition arcs to give a negative (inversely proportional) contribution. Finally, the initial marking m_0 is not depicted in the figure: it has to be described separately.

3 METHODS

3.1 Graph Preprocessing

Pathway Petri nets representations of biochemical pathways are the basis for the creation of a dataset of graphs, which will be the input of our DNN model. We made some *critical choices* about the information in the Petri nets to be preserved in our dataset. In particular, in order to let the ML method focus on the topological properties of the graphs, we decided to *omit* the following information from the Petri nets:

- Kinetic formulas;
- Multiplicities of reactants and products (i.e. arc labels);
- The initial marking m_0.

Consequently, by considering again the biochemical pathway presented in Figure 1 we have that, by removing the mentioned information from its Petri net, we obtain the result shown in Figure 2.

In order to be used by the DNN model, we reformulate the "cleaned" Petri nets models of pathways into standard graphs. Hence, we represent a biochemical pathway as a directed graph $G = \langle V_G, E_G \rangle$, where $V_G = \{v_1, v_2, \ldots, v_n\}$ is a set of nodes, and

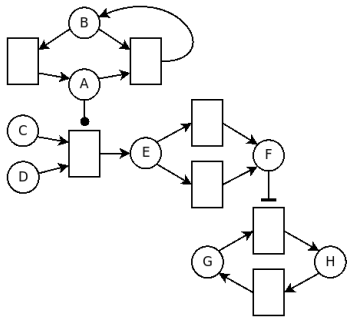

Figure 2: Pathway Petri net in which kinetic formulas and arc labels have been omitted.

$E_G = \{\langle u,v\rangle \mid u,v \in V\}$ is a set of edges. Furthermore, we define the neighborhood function of a node v as $\mathcal{N}(u) = \{v \mid (u,v) \in E_G\}$ for each node $u \in V_G$. Nodes can be of two types: *molecules*, denoted V^G_{mol}, and *reactions*, denoted V^G_{react}, with $V_G = V^G_{mol} \cup V^G_{react}$ and $V^G_{mol} \cap V^G_{react} = \emptyset$. Edges can be of three types: *standard*, denoted E^G_{std}, *promoters*, denoted E^G_{pro}, and *inhibitors*, denoted E^G_{inh}. Again, $E_G = E^G_{std} \cup E^G_{pro} \cup E^G_{inh}$ and $E^G_{std} \cap E^G_{pro} \cap E^G_{inh} = \emptyset$.

Given a pathway Petri net $N = (P,T,f,p,h,v,m_0)$ the corresponding graph G can be obtained by setting $V^G_{mol} = P$, $V^G_{react} = T$, $E^G_{std} = \{\langle u,v\rangle \in (P \times T) \cup (T \times P) \mid f(\langle u,v\rangle) > 0\}$, $E^G_{pro} = p$, $E^G_{inh} = h$. By construction, the obtained graph turns out to be bipartite. For graphs obtained in this way we adopt the same visual representation that we introduced for pathway Petri nets without kinetic formulas and arc multiplicities (see Figure 2).

Let us define G', an *enriched* version of G, as follows: initially, $V_{G'} = V_G$, $E_{G'} = E_G$. Then, if $\langle u,v\rangle \in E^G_{std}$ is a standard edge connecting a molecule to a reaction, we augment $E_{G'}$ adding the same edge but with reversed direction. Formally, we define $E^{G'}_{std} = E^G_{std} \cup \{\langle v,u\rangle \mid \langle u,v\rangle \in E^G_{std}, u \in V^G_{mol}, v \in V^G_{react}\}$. Note that we do not reverse neither standard edges from reactions to molecules, nor promotion and inhibition edges.

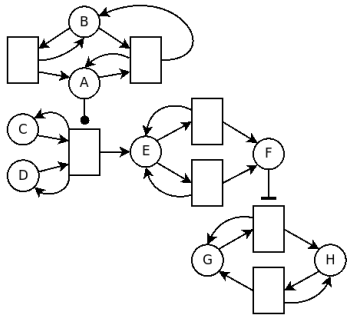

Figure 3: Enriched version of the graph in Figure 2.

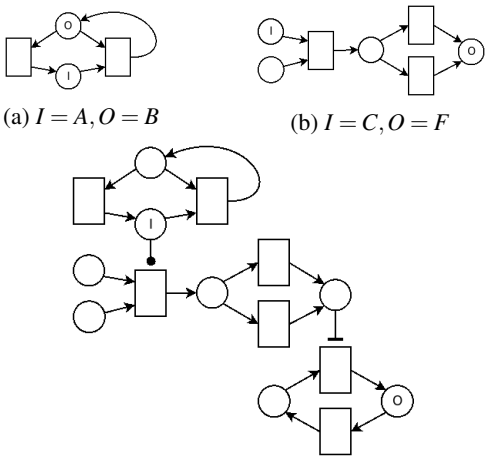

(a) $I = A, O = B$ (b) $I = C, O = F$

(c) $I = A, O = H$

Figure 4: Examples of subgraphs of the graph in Figure 2 induced by different input/output node pairs $(u,v) = (I,O)$.

The enriched version G' of the graph G obtained from the Petri net in Figure 2 is shown in Figure 3. It now represents influence relationships between molecules and reactions. There is an edge (of any type) from a molecule to a reaction if and only if a perturbation in the concentration of the molecule determines a change in the reaction rate (that should be computed from the omitted kinetic formula). Similarly, there is an edge from a reaction to a molecule if and only if a perturbation in the reaction rate determines a change in the dynamics of the concentration of that molecule. This is intuitive for edges connecting reactions to products: the dynamics of the product accumulation is determined by the reaction rate. As regards the reversed edges we added in the enriched graph, this is motivated by the fact that a perturbation in the reaction rates determines a variation in the consumption of the reactants. The enriched graph essentially corresponds to the *influence graph* that could be computed from the Jacobian matrix containing the partial derivatives of the system of ODEs of the modelled molecular pathway (Fages and Soliman, 2008).

Since we want to assess a property, concentration robustness, which expresses a relationship between an input and an output molecules of a given pathway, we can, through the enriched graph G', determine which portion of the graph modelling the pathway is relevant for the assessment of the property. Given a graph G, and a pair of nodes u and v, we define $S_{uv} = \langle V_{S_{uv}}, E_{S_{uv}}\rangle$, the *subgraph of G induced by the input/output node pair (u,v)*, informally as follows: S_{uv} is the smallest subgraph of G whose node set contains u, v, as well as nodes in every possible oriented path from u to v in G'. We remark that S_{uv} is a subgraph of G, although it is computed on the basis

of the paths in G'. Figure 4 shows some examples of induced subgraphs extracted from the graph in Figure 2. Induced subgraphs will allow us to apply the ML approach only on the portions of the graph which are relevant for the property by getting rid of unnecessary nodes and edges.

3.2 Graph Neural Networks

Traditional ML modeling assumes that the input data is represented as fixed-size, continuous vectors. In contrast, graphs are discrete objects by nature, whose size is variable. Hence, learning from graphs is not straightforward; to be exploited by ML models, graph structure, as well as information contained in nodes and edges, must be mapped jointly into a shared, real-valued vector. Of course, the effectiveness of the mapping is closely related to how much the original relationships are preserved: for example, distances between graphs in graph space should remain relatively consistent between vectors in the mapping space. GNNs are neural networks that are able to learn meaningful graph-to-vector mappings adaptively from data. The core idea of GNNs is to associate a state vector, also called *embedding*, to each node of a graph; initially, the embedding is a vector of node descriptors. Then, the embedding of each node is updated as a function of the embeddings of its neighboring nodes. We refer to this transformation as applying a GNN *layer*[2] to the node. This process can be iterated multiple times, by composing ("stacking") these layer transformations. Taking Figure 5 as a visual example, we now describe how GNNs work. Let us assume that our reference graph is composed of the node to be processed, v, and its neighboring nodes (shaded in the figure) u_1, u_2, and u_3. Suppose that we have already applied i GNN layers to the node, and $i+1$ GNN layers to its neighboring nodes. The task is to update the embedding of the current node, h_v^i, through the application of the $i+1$ GNN layer; this initial situation is shown in Figure 5a. The first operation performed by a GNN layer is *neighborhood aggregation*, shown in Figure 5b. Specifically, a neighboring function $\mathcal{N}(v)$ selects nodes (or a subset of nodes) in the neighborhood of v, and combines their embedding through a permutation-invariant[3] function Γ, producing the neighborhood vector $h_{\mathcal{N}(v)}^{i+1}$. The subsequent phase is shown in Figure 5c, in which the neighborhood vector and the current node embedding h_v^i (shown shaded in the figure) are combined together by a function Φ to obtain the updated node embedding. In its entirety, the node embedding h_v^{i+1} is computed as follows:

$$h_v^{i+1} = \sigma(w^i \cdot \Phi(h_v^i, h_{\mathcal{N}(v)}^{i+1})),$$

where σ is a non-linear function called activation, and w is a vector of "trainable" weights, whose values are tuned (usually with gradient descent) to best approximate the relationship between the input graph and the target property. Notice that each new layer reuses the embedding computed at the previous layer as its input; also, recall that the initial embedding h_v^0 is a vector of node descriptors (features). As the number of layers increases, node embeddings incorporate (through the neighborhood vector) information coming from nodes farther away: in particular, in the i-th layer, nodes receive information by nodes up to i hops from them (where a hop is defined as the shortest unweighted path between two nodes).

Once a layer is applied simultaneously to all the nodes in the graph (which corresponds to visiting each node in the graph in any order), one can produce a single embedding for the entire graph by performing *node aggregation*: that is, compute a single embedding representing the entire graph as a function of the embeddings of the graph nodes. Specifically, one can compute H_G^i, the graph embedding associated to the i-th GNN layer, by performing:

$$H_G^i = \tau(\{h_v^i \mid v \in V_G\}),$$

where τ is another permutation-invariant function called readout. Ultimately, after stacking L GNN layers, one obtains L different graph embeddings, each one constructed using information coming from a progressively "broader" view of the graph. At this point, the common practice is to concatenate all these embeddings into a single vector and obtain H_G, a final graph embedding which can be used as input by common ML algorithms for tasks such as regression or classification. Note that different choices of Γ, Φ and τ result in different GNN variants. For example, Γ and τ can be vector sum, and Φ can be simple vector concatenation, or a more complicated function approximated by a neural network. Details specific to our implementation are discussed in Section 4.2.

3.3 Model

Here, we describe our learning framework in detail. We are given a set of pathway Petri networks $\mathcal{G} = \{G_1, G_2, \ldots, G_N\}$, represented as graphs following the formulation in Section 3.1. Each graph is associated with a set of tuples $T_G : \{(S_{uv}, r) \mid u, v \in V_G, r \in$

[2] In accordance to the terminology of DNNs, where layers are functions that apply a data-driven transformation to their inputs (Goodfellow et al., 2016).

[3] A function f is invariant with respect to a permutation π iff $f(x) = f(\pi(x))$; in our case, the input x are sets of node embeddings.

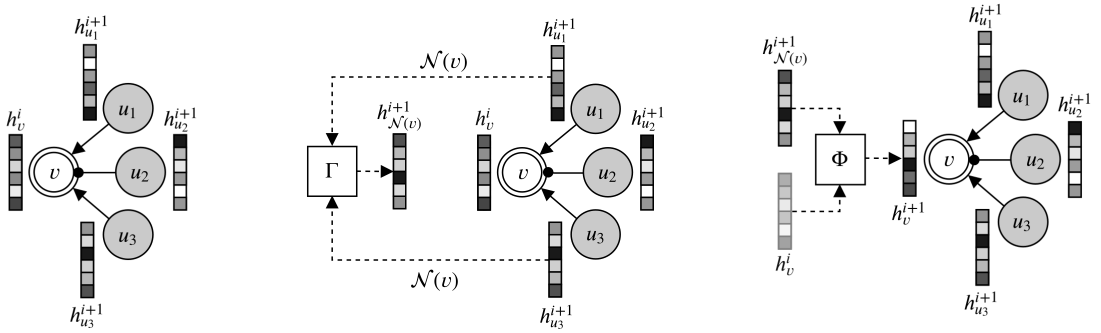

(a) Initial graph (b) Neighbor aggregation (c) Embedding update (weight multiplication and non-linearity not shown).

Figure 5: An example of GNN processing at the node level.

$[0,1] \subseteq \mathbb{R}\}$, where u and v are graph nodes, S_{uv} is their induced subgraph, and r expresses how much the output node v is robust to perturbations to the input node v. Note that our task is to learn to predict whether the induced subgraph associated to a pair of input/output nodes is robust or not, as opposed to learn the exact value of the property. Hence, in ML terms, we tackle a classification problem where our graph labels belong to the discrete set $\{0,1\}$, with 0 indicating not robust, and 1 indicating robust. It is straightforward to transition from the original problem to a classification one by simply discretizing robustness values into indicators as follows:

$$t = \begin{cases} 1 & \text{if } r > 0.5 \\ 0 & \text{otherwise.} \end{cases}$$

Our reference set thus becomes: $T_G : \{(S_{uv}, t) \mid u, v \in V_{mol}^G, t \in \{0,1\}\}$. As additional notation, we will refer to 1 as the "positive class", and 0 as the "negative class". Having collected all the necessary information, we build a dataset of induced subgraphs and their associated robustness indicators $\mathcal{D} = \bigcup_{G \in \mathcal{G}} \{T_G\}$. With this premise, our predictive task is the following: given a previously unseen pathway network and a pair of input/output species nodes, we seek to predict the associated robustness indicator with reasonable accuracy. In our graph framework, this corresponds to learn a function $f(S_{uv}) = \hat{t}$ that given an induced graph S_{uv} over nodes u and v, predicts a robustness value $\hat{t}$ which is as close as possible to the ground truth t, i.e. we wish to minimize the following binary cross-entropy (Janocha and Czarnecki, 2017) (BCE) objective function:

$$\text{BCE}(\mathcal{D}) = -\frac{1}{M} \sum_{T_G \in \mathcal{D}} \sum_{S,t \in T_G} t \, \log(\hat{t}) + (1-t)\log(1-\hat{t}),$$

with $M = |\mathcal{D}| \cdot |T_G|$, where we drop the subscript notation on S for ease of notation. We propose to approximate f using a DNN composed of a GNN that receives as input an induced subgraph S (defined over a certain input/output node pair (u,v)), and produces as output an embedding H_S. This embedding is taken as input by an MLP classifier, which outputs a value between 0 and 1. The DNN output can be interpreted as the probability of v being robust to perturbations in u, given the structural information of the induced subgraph. The corresponding predicted indicator can be obtained by simply rounding this probability to the nearest integer. More formally, we estimate the unknown function f with the following:

$$f(S) \approx \text{MLP}_\phi(H_S),$$

where H_S is the induced subgraph embedding obtained by the GNN in a similar fashion as described in Section 3.2, and ϕ are weights that are learned using gradient descent. Figure 6 shows a high-level overview of our model.

4 EXPERIMENTS

4.1 Dataset Construction

Our dataset originates from 706 SBML models of biochemical pathways downloaded from the BioModels database (Le Novere et al., 2006). They correspond to the complete set of manually curated models present in the database at the time we started the construction of the dataset[4]. From these models, we built the associated Petri nets representations, which were saved as graphs in DOT format[5]. For the translation of the SMBL models into (pathway) Petri nets we developed a Python script that, for each reaction in the SMBL

[4]May 2019.

[5]The DOT graph description language specification, available at: https://graphviz.gitlab.io/_pages/doc/info/lang.html

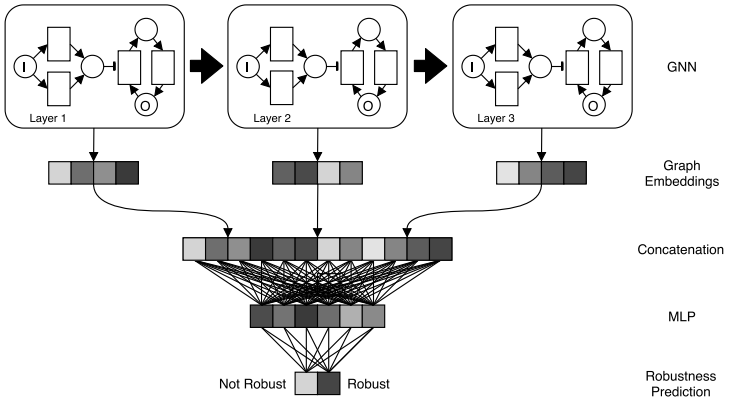

Figure 6: A high-level overview of our model to predict robustness (using three GNN layers for ease of visualization). The big black arrow connecting layers indicates that node states computed at layer i are used to initialize layer $i+1$. Note how each layer computes a different graph embedding (where color intensity is used as a proxy for value magnitude).

model extracts reactants, products and modifiers. It also checks the kinetic formula in order to determine whether each modifier is either promoter or an inhibitor. Subsequently, empty graphs (not containing any node) and duplicates were discarded. The remaining ones were translated into graphs compliant with the notation described in Section 3.1, and the corresponding induced subgraphs for each input/output combination were extracted. At this point, in order to have a size-homogeneous dataset of graphs and since we did not have any previous knowledge of the effectiveness of GNNs on this task, we focused on induced subgraphs with at most 40 nodes. We plan to extend our results to larger graphs in future works. After this preprocessing, we ended up with a dataset of 7013 induced subgraphs.

The robustness values to be used as labels of the induced subgraphs have been computed by following the relative α-robustness approach. The dynamics of each biochemical pathway has been simulated by applying a numerical solver (the `libRoadRunner` Python library) to its ODEs representation. Reference initial concentrations of involved molecules have been obtained from the original SBML model of each pathway. Moreover, 100 simulations have been performed for each molecule of the pathway by perturbing its initial concentration in the range $[-20\%, +20\%]$. The termination of each simulation has been set to the achievement of the steady state, with a timeout of 250 simulated time units.[6] For each couple of input/output molecules, we computed the width α of the range of concentrations reached by the output molecules by varying the input (α-robustness). A relative robustness $\overline{\alpha}$ has then been obtained by dividing α by the concentration reached by the output when the initial concentration of the input is the reference one (no perturbation). Finally, a robustness value $r \in [0,1]$ to be used in the dataset has been computed by comparing $\overline{\alpha}$ (a relative representation of the output range) with 0.4 (a relative representation of the initial input range, that is 40%). Formally:

$$r = 1 - min(1, \frac{\overline{\alpha}}{0.4})$$

4.2 Model Implementation Details

We set up the initial node embeddings as a binary feature vector of size 3. The first position encodes whether the corresponding node is a molecule species (with value 1), or a reaction (with value 0). The second position encodes whether the node is an input species (with value 1) or not. The third position encodes whether the node is an output species (with value 1) or not. As regards the GNN, we follow the seminal approach in (Kipf and Welling, 2017), which uses element-wise mean as Γ, and vector sum as Φ. Since edges can be of different types (three in our case), we implemented the following variant of the general GNN formulation:

$$h_v^{i+1} = \sigma(\sum_{k \in K} w_k^i \cdot \Phi(h_v^i, h_{\mathcal{N}(v,k)}^i)),$$

where $\mathcal{N}(v,k)$ is an edge-aware neighborhood function that selects only neighboring nodes of v connected by an edge of type k, with K as the set of possible edge types. In other words, neighborhood aggregation is repeated once for each edge type; the corresponding results are multiplied by a specific edge-type weight matrix and summed together. This way, the network can separately learn the contributions of

[6] The concentration values obtained at the end of the simulation are considered as steady state values also in the cases in which the timeout has been reached.

each different edge type. As activation function σ, we used Rectified Linear Units (ReLU) (Glorot et al., 2011). As regards the MLP used for the final classification, it is composed of two linear layers followed by ReLU non-linearities and a final linear layer that maps its input to the output space. Moreover, intermediate layers are regularized with Dropout (Srivastava et al., 2014), with drop probability 0.1. In our experiments, we optimize the number of GNN layers L, choosing in the set $\{1,2,\ldots,8\}$; the type of node aggregation (i.e. the τ function), choosing among element-wise sum, mean or max; and the dimension of the node state vector after the first layer, choosing between 64 and 128. The selection of the hyper-parameters is explained in more detail in Section 4.3. The model has been implemented in Python, using the `PyTorch Geometric` (Fey and Lenssen, 2019) library.

4.3 Evaluation

We evaluate the accuracy of the proposed model using 5-fold Cross-Validation (CV). In more detail, the dataset is divided into 5 partitions of equal size. Each partition is further split in three: the first partition (80% of the partition size) is used as training set to optimize the model parameters with gradient descent, whose values are tuned according to the task and the data at hand, as discussed in Section 3.3. Our optimizer of choice is Adam (Kingma and Ba, 2015), with a learning rate of 0.001. The second (%10 of the partition size) is used as validation set to choose the optimal values of the hyper-parameters, among 8 possible number of GNN layers, 3 possible node aggregating functions and 2 possible node embedding dimensions. In particular, we instantiate 48 models, one for each possible combination of the hyper-parameter values (see Section 4.2), and record their accuracy on the validation set; we then choose as best model the one with the highest validation accuracy. The third (%10 of the partition size) is used as independent test set to evaluate the best model, and compute an unbiased estimate of its out-of-sample accuracy. This procedure is repeated for each partition; ultimately, it results in 5 estimates which are averaged to compute the final test accuracy. Notice that this procedure does not use data already "seen" by the model, either during training or validation, to assess its performance. Importantly, we noticed a class imbalance in favour of robust graphs; in fact, approximately 73% of subgraphs were labelled with the positive class. Hence, only during model training, we oversampled the minority class and trained the model with an equal number of positive and negative examples. Our experiments required 3 days of computation on a single Tesla M40 GPU.

5 RESULTS

Figure 7a reports the accuracy obtained by our model, averaged over the 5 test partitions, where the first four rows display the accuracy stratified according to the number of nodes of subgraphs in the test set. To show the effectiveness of our method, we compare against a baseline that predicts the most frequent class in the test set, which we term the Null model. Note that, due to label stratification, class proportions are equal in all 5 test partitions, thus the overall accuracy of the Null model is the same in all folds; indeed, the associated standard deviation is 0. As can be seen, our model consistently outperforms the baseline in all considered strata. Figure 7b shows the confusion matrix obtained by the model over the entire dataset, emphasizing the positive results of our model. As additional information, we report that our model obtained an overall sensitivity of 0.7873 ± 0.0756 and an overall specificity of 0.8992 ± 0.0121.

The table also highlights that our model performs better when predicting graphs with a large number of nodes. In particular, for graphs with number of nodes ranging from 21 to 30, the model obtains the best predictive performance (over 93%), while for the largest graphs (31-40 nodes), it obtains the highest improvement with respect to the baseline (approximately 20%). This trend is shown more clearly in Figure 7c, where we plot the improvement in accuracy as the number of nodes increases, using a sliding window of size 10 to smooth the effect of outliers.

The lower prediction accuracy in the case of small graphs (1-10 nodes) can be explained by observing that we trained the model on a dataset of graphs in which kinetic, stoichiometric and initial concentration parameters have been omitted. The smaller is the graph, the higher is, in general, the influence on its dynamics of these parameters. For example, let us consider again the biochemical pathway introduced in Figure 1 and the corresponding graph depicted in Figure 2. Moreover, let us consider the following kinetic and initial concentration (marking) parameters:

$$k1 = 1.0 \quad k3 = 0.01 \quad k5 = 0.01 \quad k7 = 0.3$$
$$k2 = 5.0 \quad k4 = 0.1 \quad k6 = 5.0$$

$$m_0(A) = 50 \quad m_0(D) = 100 \quad m_0(G) = 100$$
$$m_0(B) = 50 \quad m_0(E) = 0 \quad m_0(H) = 0$$
$$m_0(C) = 100 \quad m_0(F) = 0$$

On the basis of numerical simulations of the ODEs in Figure 1b we obtained, by varying the initial concentration of each molecule in the interval $[-20\%, +20\%]$ the robustness values presented in Table 1. In Table 2, we list the average and standard deviations of the 5 different models evaluated in Sec-

# Nodes (# subgraphs)	Model	Null
1-10 (685)	**0.7456** $\pm$ 0.0455	0.6385 $\pm$ 0.0213
11-20 (2679)	**0.8625** $\pm$ 0.0091	0.7327 $\pm$ 0.0207
21-30 (1690)	**0.9350** $\pm$ 0.0136	0.8384 $\pm$ 0.0267
31-40 (1959)	**0.8645** $\pm$ 0.0303	0.6683 $\pm$ 0.0105
Overall (7013)	**0.8692** $\pm$ 0.0140	0.7322 $\pm$ 0.0000

(a) Overall and stratified accuracies.

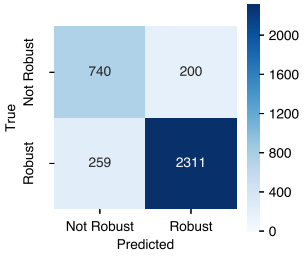

(b) Confusion Matrix.

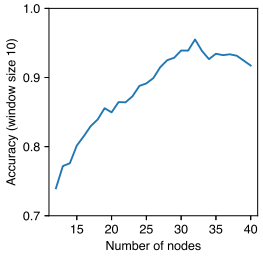

(c) Accuracy improvement plot.

Figure 7: Results of the proposed model.

Table 1: Robustness values computed by numerical simulation of the ODEs in Figure 1b. Input molecules with initial concentration equal to 0 are omitted. Output molecules with identical robustness values are merged.

Input	Output				
	A	**B**	**C/D**	**E/F**	**G/H**
A	1.0	0.73	0.99	1.0	1.0
B	1.0	0.73	0.99	1.0	1.0
C	1.0	1.0	0.0	0.99	0.99
D	1.0	1.0	0.0	0.99	0.99
G	1.0	1.0	1.0	1.0	0.5

Table 2: Probabilities of robustness obtained from the model for some relevant input/output combinations.

Input	Output	Probability
B	A	0.8092 $\pm$ 0.1493
A	F	0.9906 $\pm$ 0.0187
A	H	1.0000 $\pm$ 0.0000
C	F	0.2398 $\pm$ 0.2697
G	H	0.2620 $\pm$ 0.0272

tion 4.3, when tasked to predict the robustness probabilities of some relevant input/output combinations. We remark that values in the two tables are not directly comparable: those in Table 1 are exact robustness values of this specific example while those in Table 2 are probabilities of the robustness values to be greater than 0.5 (averaged across 5 models). In this specific case the prediction turns out to be accurate in the case of input/output pairs corresponding to big induced subgraphs. This happens in the cases of input A with output F or H. The prediction seems not correct in the case of input C and output F: the models gives a small probability while ODEs simulations give 0.99. We notice that the robustness value of this input/output combination is actually sensitive to the perturbation of parameters that have been omitted in the dataset. In particular, if the initial concentration of C, which was omitted in the dataset, was 80 instead of 100, the robustness value with input C and output F would become 0.5 rather than 0.99.

The prediction turns out to be rather correct also in the case of input B and output A. It it interesting to observe that the probability is high, but not very close to 1. Indeed, also in this case the robustness is influenced by parameters that are not taken into account in the dataset, such as the label of the arc entering in node B. Finally, in the case of input G and output H the prediction gives a small probability of robustness and indeed the actual measured value is borderline (0.5).

6 CONCLUSIONS

The experimental results we obtained show that our model can infer topological properties of graphs which correlate with dynamical properties of the corresponding biochemical pathways. Such results, although still preliminary, are promising and let us believe that the approach deserves further investigation. Indeed, the assessment of new connections between structural and dynamical properties of biochemical pathways, and the development of automatic methods for their inference, could lead to new and more efficient ways of studying the functioning of living cells.

Moreover, we want to emphasize the fact that, once trained, the time needed to obtain a prediction from the DNN is in the order of milliseconds, while performing numerical simulations can be orders of magnitude slower (the simulation of most of the considered models took times in the order of minutes, bigger models in the order dozens of minutes or hours). The bulk of the computational cost of DNN models is placed on the training phase, which however needs to be performed only once. For this reason we think that, once perfected, methods inspired by our approach have the potential of enabling faster advances in the field.

The efficiency of our approach is based on the aim of replacing numerical simulations with the assess-

ment of structural properties of pathways. Such an assessment is performed by the DNN model. It is difficult to imagine how the same assessment could be done through an algorithm on graphs since the structural properties to be assessed are not known in advance, but inferred.

In order to consolidate the results we obtained, as future work we plan to extend the investigation of robustness to a dataset in which also very large graphs (> 40 nodes) are included. On one hand, this will be challenging from a computational point of view, because some biological networks included in the original dataset comprise a number of nodes in the order of hundreds and thousands. On the other, having a large dataset will probably be beneficial to our model, since the effectiveness of Deep Neural Networks is generally proportional to the number of training examples. Another line of research to pursue concerns model explainability. Indeed, our DNN has thousands of parameters, which make explaining the "why" behind their predictions (i.e. which parts of the pathway contributed to the prediction, and to what extent) a hard task. Motivated by this challenge, we plan to develop generative models of pathway networks to work towards the goal of making these models explainable.

Furthermore, we will consider enriching the dataset with information we have omitted in the present study. In particular, we may include arc labels (multiplicities of reactants/products) in order to evaluate their significance. Moreover, we may include something about kinetic formulas, such as their parameters (properly normalized). The latter addition could, in principle, improve the accuracy of the model on small subgraphs, but its effect on the accuracy of big ones has to be carefully evaluated.

Lastly, we plan to apply the approach to the assessment of other dynamical properties such as other notions of robustness as well as, for example, monotonicity, oscillatory and bistability properties.

ACKNOWLEDGEMENTS

This work has been supported by the project "Metodologie informatiche avanzate per l'analisi di dati biomedici" funded by the University of Pisa (PRA 2017_44).

AUTHORS' CONTRIBUTION

The four authors contributed equally to this work.

REFERENCES

Fages, F. and Soliman, S. (2008). From reaction models to influence graphs and back: A theorem. In Fisher, J., editor, *Formal Methods in Systems Biology*, pages 90–102, Berlin, Heidelberg. Springer Berlin Heidelberg.

Fey, M. and Lenssen, J. E. (2019). Fast graph representation learning with PyTorch Geometric. In *ICLR Workshop on Representation Learning on Graphs and Manifolds*.

Gilbert, D., Heiner, M., and Lehrack, S. (2007). A unifying framework for modelling and analysing biochemical pathways using petri nets. In Calder, M. and Gilmore, S., editors, *Computational Methods in Systems Biology*, pages 200–216, Berlin, Heidelberg. Springer Berlin Heidelberg.

Gillespie, D. T. (1977). Exact stochastic simulation of coupled chemical reactions. *The journal of physical chemistry*, 81(25):2340–2361.

Glorot, X., Bordes, A., and Bengio, Y. (2011). Deep sparse rectifier neural networks. In *Proceedings of the Fourteenth International Conference on Artificial Intelligence and Statistics*, pages 315–323.

Goodfellow, I., Bengio, Y., and Courville, A. (2016). *Deep Learning*. The MIT Press.

Gori., R., Milazzo., P., and Nasti., L. (2019). Towards an efficient verification method for monotonicity properties of chemical reaction networks. In *Proceedings of the 12th International Joint Conference on Biomedical Engineering Systems and Technologies - Volume 3: BIOINFORMATICS,*, pages 250–257. INSTICC, SciTePress.

Hucka, M., Bergmann, F. T., Dräger, A., Hoops, S., Keating, S. M., Le Novère, N., Myers, C. J., Olivier, B. G., Sahle, S., Schaff, J. C., et al. (2018). The systems biology markup language (sbml): language specification for level 3 version 2 core. *Journal of integrative bioinformatics*, 15(1).

Iooss, B. and Lemaître, P. (2015). A review on global sensitivity analysis methods. In *Uncertainty management in simulation-optimization of complex systems*, pages 101–122. Springer.

Janocha, K. and Czarnecki, W. (2017). On loss functions for deep neural networks in classification. *Schedae Informaticae*, 25.

Karp, P. D. and Paley, S. M. (1994). Representations of metabolic knowledge: pathways. In *Ismb*, volume 2, pages 203–211.

Kingma, D. P. and Ba, J. (2015). Adam: A method for stochastic optimization. In *Proceedings of the 3rd International Conference on Learning Representations*, ICLR.

Kipf, T. N. and Welling, M. (2017). Semi-supervised classification with graph convolutional networks. In *5th International Conference on Learning Representations, ICLR*.

Kitano, H. (2004). Biological robustness. *Nature Reviews Genetics*, 5(11):826.

Kitano, H. (2007). Towards a theory of biological robustness. *Molecular systems biology*, 3(1).

Larhlimi, A., Blachon, S., Selbig, J., and Nikoloski, Z. (2011). Robustness of metabolic networks: a review of existing definitions. *Biosystems*, 106(1):1–8.

Le Novere, N., Bornstein, B., Broicher, A., Courtot, M., Donizelli, M., Dharuri, H., Li, L., Sauro, H., Schilstra, M., Shapiro, B., et al. (2006). Biomodels database: a free, centralized database of curated, published, quantitative kinetic models of biochemical and cellular systems. *Nucleic acids research*, 34(suppl_1):D689–D691.

Le Novere, N., Hucka, M., Mi, H., Moodie, S., Schreiber, F., Sorokin, A., Demir, E., Wegner, K., Aladjem, M. I., Wimalaratne, S. M., et al. (2009). The systems biology graphical notation. *Nature biotechnology*, 27(8):735.

Li, C., Donizelli, M., Rodriguez, N., Dharuri, H., Endler, L., Chelliah, V., Li, L., He, E., Henry, A., Stefan, M. I., Snoep, J. L., Hucka, M., Le Novère, N., and Laibe, C. (2010). BioModels Database: An enhanced, curated and annotated resource for published quantitative kinetic models. *BMC Systems Biology*, 4:92.

Micheli, A. (2009). Neural Network for Graphs: A Contextual Constructive Approach. *Trans. Neur. Netw.*, 20(3):498–511.

Murtagh, F. (1991). Multilayer perceptrons for classification and regression. *Neurocomputing*, 2(5):183–197.

Nasti, L., Gori, R., and Milazzo, P. (2018). Formalizing a notion of concentration robustness for biochemical networks. In *Federation of International Conferences on Software Technologies: Applications and Foundations*, pages 81–97. Springer.

Peterson, J. L. (1977). Petri nets. *ACM Computing Surveys (CSUR)*, 9(3):223–252.

Reddy, V. N., Mavrovouniotis, M. L., Liebman, M. N., et al. (1993). Petri net representations in metabolic pathways. In *ISMB*, volume 93, pages 328–336.

Rizk, A., Batt, G., Fages, F., and Soliman, S. (2009). A general computational method for robustness analysis with applications to synthetic gene networks. *Bioinformatics*, 25(12):i169–i178.

Scarselli, F., Gori, M., Tsoi, A. C., Hagenbuchner, M., and Monfardini, G. (2009). The Graph Neural Network Model. *Trans. Neur. Netw.*, 20(1):61–80.

Shinar, G. and Feinberg, M. (2010). Structural sources of robustness in biochemical reaction networks. *Science*, 327(5971):1389–1391.

Somogyi, E. T., Bouteiller, J.-M., Glazier, J. A., König, M., Medley, J. K., Swat, M. H., and Sauro, H. M. (2015). libroadrunner: a high performance sbml simulation and analysis library. *Bioinformatics*, 31(20):3315–3321.

Srivastava, N., Hinton, G., Krizhevsky, A., Sutskever, I., and Salakhutdinov, R. (2014). Dropout: A simple way to prevent neural networks from overfitting. *Journal of Machine Learning Research*, 15:1929–1958.

Zi, Z. (2011). Sensitivity analysis approaches applied to systems biology models. *IET systems biology*, 5(6):336–346.